Structure and function of an insect α-carboxylesterase (α*Esterase*7) associated with insecticide resistance

Colin J. Jackson[a,b,1], Jian-Wei Liu[c], Paul D. Carr[a], Faisal Younus[c], Chris Coppin[c], Tamara Meirelles[a], Mathilde Lethier[b], Gunjan Pandey[c], David L. Ollis[a], Robyn J. Russell[c], Martin Weik[b], and John G. Oakeshott[c]

[a]Research School of Chemistry, Australian National University, Canberra, ACT 0200, Australia; [b]Institut de Biologie Structurale, Commissariat a l'Energie Atomique, F-38027 Grenoble, France; and [c]Commonwealth Scientific and Industrial Research Organization (Australia) Ecosystems Science, Canberra, ACT 0200, Australia

Edited by Bruce D. Hammock, University of California, Davis, CA, and approved May 2, 2013 (received for review March 6, 2013)

Insect carboxylesterases from the *αEsterase* gene cluster, such as αE7 (also known as E3) from the Australian sheep blowfly *Lucilia cuprina* (*Lc*αE7), play an important physiological role in lipid metabolism and are implicated in the detoxification of organophosphate (OP) insecticides. Despite the importance of OPs to agriculture and the spread of insect-borne diseases, the molecular basis for the ability of α-carboxylesterases to confer OP resistance to insects is poorly understood. In this work, we used laboratory evolution to increase the thermal stability of *Lc*αE7, allowing its overexpression in *Escherichia coli* and structure determination. The crystal structure reveals a canonical α/β-hydrolase fold that is very similar to the primary target of OPs (acetylcholinesterase) and a unique N-terminal α-helix that serves as a membrane anchor. Soaking of *Lc*αE7 crystals in OPs led to the capture of a crystallographic snapshot of *Lc*αE7 in its phosphorylated state, which allowed comparison with acetylcholinesterase and rationalization of its ability to protect insects against the effects of OPs. Finally, inspection of the active site of *Lc*αE7 reveals an asymmetric and hydrophobic substrate binding cavity that is well-suited to fatty acid methyl esters, which are hydrolyzed by the enzyme with specificity constants (~10^6 M^{-1} s^{-1}) indicative of a natural substrate.

protein engineering | directed evolution | ali-esterase

The demand for greater productivity from agriculture and the avoidance of insect-borne diseases has made efficient control of insect pests increasingly important; in 2007, the world market for insecticides was estimated to be in the order of $11 billion US (1). However, the effectiveness of insecticides is decreasing, with over 500 documented instances of insecticide resistance (2). The development of resistance to organophosphate (OP) (Fig. 1*A*) pesticides through the action of α-carboxylesterases (α-CBEs) has been documented in many species (3), including the Australian sheep blowfly *Lucilia cuprina* (4). OPs inhibit acetylcholinesterase (AChE) at cholinergic synapses in the central and peripheral nervous systems, which leads to interminable nerve signal transduction and death (5). However, α-CBEs, such as αE7 in *L. cuprina* (*Lc*αE7), confer a significant protective effect on insects owing to their ability to bind and slowly hydrolyze OPs (6). It has also been shown that this CBE-mediated OP resistance can be increased through G137D and W251L point mutations (4, 7).

Insect α-CBEs, including *Lc*αE7, are thought to play important physiological roles in lipid and xenobiotic metabolism (6, 8). They are one of the most abundant protein families in insects, with between 20 and 40 active CBEs predicted to be expressed by the fruit fly *Drosphila melanogaster* (9, 10). Although the physiological substrates of insect α-CBEs are unknown, recent MS results have shown that *D. melanogaster* αE7 is expressed in the fat body lipid droplet proteome (11), implying a role in lipid or cholesterol metabolism. This work has been extended to show that *D. melanogaster* αE7-null mutants exhibit reduced lifespan, lowered insecticide tolerance, and reduced lipid storage capacity (6).

Intense efforts over the last 50 y have shed light on the critical role that CBEs have played in the evolution of insecticide resistance (12). However, in the absence of a molecular structure of an insect CBE, the interactions of these enzymes with pesticides or natural substrates and the effects of mutations and sequence polymorphisms could not be understood at a molecular level. In this work, we describe the directed evolution of *Lc*αE7 for increased stability and heterologous expression in *Escherichia coli*, which allowed us to grow crystals and solve the structure. By soaking crystals of *Lc*αE7 in OPs, we have been able to capture it in its phosphorylated state after OP hydrolysis, allowing us to understand the structural features that confer insecticide resistance to the fly. Finally, this structure allowed us to identify the probable natural substrate for these enzymes.

Results and Discussion

Evolving a Stable Variant of *Lc*αE7 for Structure Determination. Previous attempts to purify and crystallize WT *Lc*αE7 have been hampered by the instability of the protein, and therefore, we performed a laboratory (directed) evolution experiment to increase its stability and allow its overexpression in *E. coli*. This process involved successive rounds of mutagenesis of the gene using error-prone PCR before the variants were screened for increased thermal stability. Approximately 100,000 random variants of *Lc*αE7 were plated onto agar plates and then replica-plated onto filter paper, which was incubated at various temperatures for 1 h. After incubation, the filter paper was immersed in a solution of the model ester substrate 2-naphthyl acetate and fast-red dye, which forms a red complex with the naphthol product of hydrolysis. Colonies that displayed the greatest activity were selected as positive clones and pooled for the next round of random mutagenesis. After four rounds, an enhanced variant was obtained that contained six mutations (M364L, I419F, A472T, I505T, K530E, and D554G). Bacterial colonies in which this variant was expressed displayed significant esterase activity after incubation at 54 °C for 1 h, whereas colonies expressing the WT enzyme displayed no activity after this heat treatment.

The best *Lc*αE7 variant, hereafter termed *Lc*αE7-4, was purified from *E. coli*. Measurement of its thermal stability and comparison with WT *Lc*αE7 confirmed that the mutations provided stabilizing effects. Specifically, we observed a 5.6 °C increase in the apparent temperature at which the protein lost one-half of its activity through thermal denaturation (Tm_{50}^{app}; from 41.9 °C in the WT to 47.5 °C in *Lc*αE7-4) (Fig. S1). The kinetic parameters of *Lc*αE7-4 were very similar to the parameters of the WT enzyme (k_{cat}/K_M = 1.1 × 10^6 s^{-1} M^{-1} vs. 1.8 × 10^6 s^{-1} M^{-1}),

Author contributions: C.J.J., J.-W.L., D.L.O., R.J.R., M.W., and J.G.O. designed research; C.J.J., J.-W.L., P.D.C., F.Y., C.C., T.M., M.L., and G.P. performed research; C.J.J., M.W., and J.G.O. analyzed data; and C.J.J. and J.G.O. wrote the paper.

The authors declare no conflict of interest.

This article is a PNAS Direct Submission.

Freely available online through the PNAS open access option.

Data deposition: The crystallography, atomic coordinates, and structure factors have been deposited in the Protein Data Bank, www.pdb.org (PDB ID codes 4FG5, 4FNG, and 4FNM).

[1]To whom correspondence should be addressed. E-mail: cjackson@rsc.anu.edu.au.

This article contains supporting information online at www.pnas.org/lookup/suppl/doi:10.1073/pnas.1304097110/-/DCSupplemental.

BIOCHEMISTRY

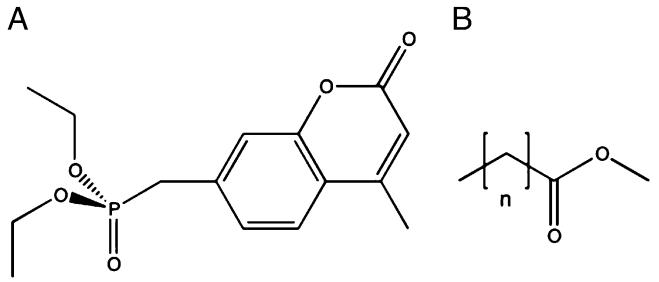

Fig. 1. Chemical structures of the substrates used in this work. (*A*) The OP diethyl-4-methylumbelliferyl phosphate (DEUP). (*B*) The generic structure of FAMEs. Hexanoate, $n = 4$; octanoate, $n = 6$; decanoate, $n = 8$; laurate, $n = 10$; myristate, $n = 12$.

suggesting that the mutations have not significantly affected the structure.

Size exclusion chromatography revealed that *Lc*αE7-4 existed in equilibrium between monomeric and dimeric forms (Fig. S2). Each of these peaks was concentrated to 8 mg/mL and screened for crystallization. Crystals of both the monomeric and the dimeric forms of the enzyme were obtained and diffracted to 2.2 and 1.95 Å, respectively (Table 1). The structure was solved by molecular replacement using the structure of mouse AChE (13), which shares 29% amino acid identity. Several AChE structures were used in the molecular replacement search, with this structure being the only one to give a correct solution. There were no significant differences between the monomeric and dimeric structures.

Overall Structure of *Lc*αE7. *Lc*αE7 adopts an α/β-hydrolase superfamily fold (14), which is shown in Fig. 2*A*. The canonical core of the α/β-hydrolase fold is present as well as the conserved catalytic Ser-His-Glu triad. In addition to eight canonical β-strands, the central β-sheet in *Lc*αE7 also contains two antiparallel β-strands at the start and two antiparallel β-strands at the end. The six canonical α-helices are also present, although in some instances (α-b, α-d, and α-f), additional short helices are also present. The structure diverges significantly from the canonical α/β-hydrolase fold with the presence of a large α-helix at the N terminus, which will be discussed in detail later, and two large subdomains on either side of the active site cleft on the upper face of the protein. Subdomain 1 is formed by a short antiparallel β-sheet insertion after β1, two α-helices inserted after β3, and four α-helices inserted after β6. Subdomain 2 is comprised of four α-helices inserted after β7 and two α-helices at the C terminus of the protein (Fig. 2*A*).

The monomeric and dimeric *Lc*αE7 protein structures were analyzed by the PISA server (http://www.ebi.ac.uk/msd-srv/prot_int/cgi-bin/piserver) (15). The total surface area buried at the dimer interface is 2,040 $Å^2$, which is predicted to result in free energy of dimer formation of −7.4 kcal/mol and free energy of dissociation ΔG^{diss} of 0.9 kcal/mol. The relatively small energy barrier to dissociation is consistent with its equilibrium with monomeric protein (Fig. S2). The dimer interface, which is symmetrical, is formed by subdomains 1 and 2 and dominated by symmetrical interactions between subdomain 1 from each monomer (Fig. S3).

Of six mutations that were found in the stabilized variant, three mutations (Ile419Phe, Ala472Thr, and Ile505Thr) are in the interior of the protein, and three mutations (Met364Leu, Lys530Glu, and Asp554Gly) are on its surface (Fig. S4). It is clear that the Ile419Phe mutation results in a hydrophobic cavity in the interior of the protein being filled, which is a common and established mode of protein stabilization (16). However, the other mutations do not obviously conform to established modes of protein stabilization.

N-Terminal Membrane Anchor. Analysis of the structure of *Lc*αE7 shows the presence of an amphipathic α-helix at the N terminus (Fig. 2 *A* and *B*). α-CBEs have long been known to be associated with the microsomal fraction (17). However, it was unknown how this association was maintained at a structural level. The crystal structure presented here provides an explanation: the N-terminal helix of *Lc*αE7 is rich in positively charged and hydrophobic amino acids, with an amphipathic distribution that is ideal for membrane association. This conclusion is supported by sequence analysis from the Mempype server (18), which predicted the protein to be associated with the intracellular membrane through the N-terminal helix. The helix is packed only loosely against the body of the protein in the crystal structure through hydrophobic interactions, which will allow it to easily dissociate.

Table 1. Data collection and refinement statistics for structures reported in this work

	Apo-*Lc*αE7 $P2_1$	Apo-*Lc*αE7 $C222_1$	DEUP+*Lc*αE7 $C222_1$
Space group	P1 21 1	C 2 2 21	C 2 2 21
Unit cell parameters			
a (Å)	61.77	48.62	50.65
b (Å)	108.96	100.51	102.74
c (Å)	92.17	221.74	226.40
β (°)	90.36		
Data collection			
Wavelength (Å)	0.8266	0.9393	0.8266
Resolution range (Å)*	46.9–2.19 (2.31–2.19)	19.7–1.95 (2.00–1.95)	42.5–1.80 (1.85–1.80)
No. of unique reflections	62,125	40,150	54,447
Redundancy	3.3 (3.2)	6.6 (5.7)	7.3 (6.7)
Completeness (%)	97.9 (100)	99.8 (100.0)	99.1 (97.5)
$R_{merge(I)}$	0.093 (0.439)	0.076 (0.631)	0.109 (0.60)
Mean $<I/\sigma(I)>$	12.7 (4.0)	17.6 (2.7)	15.6 (3.0)
Refinement			
No. reflections (total)	58,544	40,152	54,447
Resolution range	46.9–2.19 (2.24–2.19)	19.7–1.95 (2.02–1.95)	42.5–1.80 (1.83–1.80)
R_{work}/R_{free}	17.06/20.91 (23.7/28.3)	17.75/22.50 (24.83/32.60)	16.96/20.45 (21.54/21.86)
rmsd			
Bond lengths (Å)	0.020	0.008	0.006
Bond angles (°)	2.24	1.09	1.04
Protein Data Bank ID code	4FG5	4FNG	4FNM

*Values in parenthesis are for the highest-resolution shell.

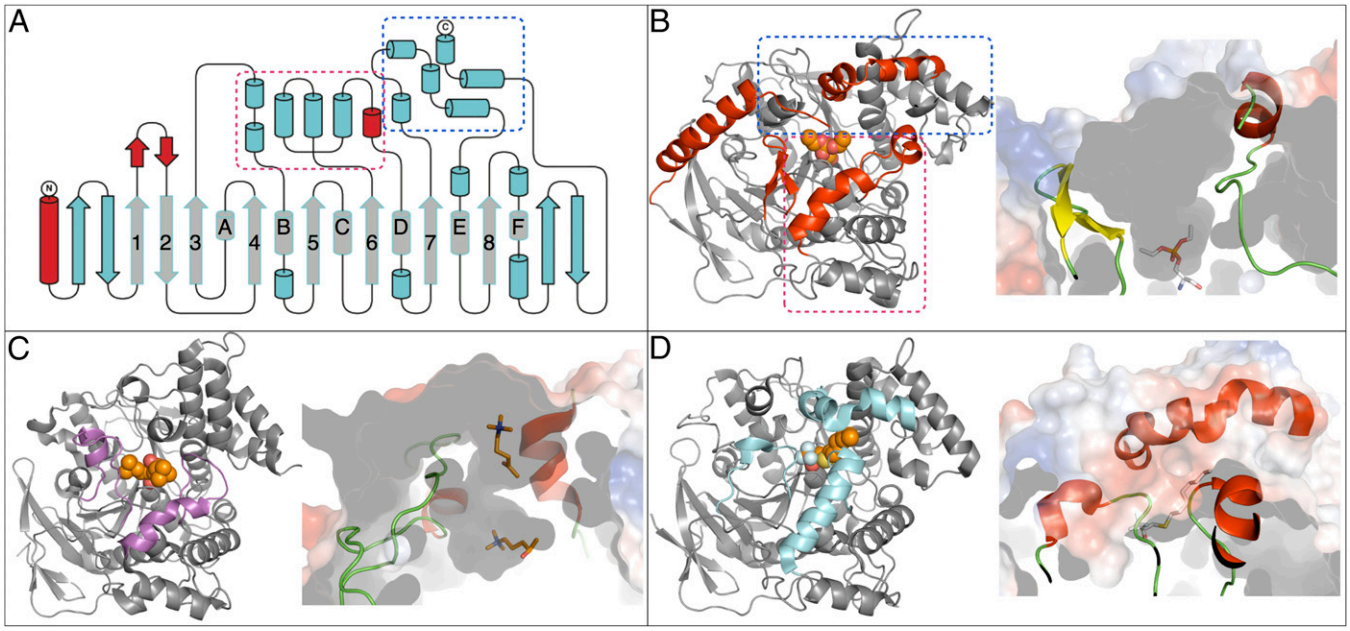

Fig. 2. (*A* and *B*) Cartoon and topology diagrams of *Lc*αE7 and comparison with (*C*) AChE and (*D*) JHE. (*A*) Topology representation of the *Lc*αE7 structure highlighting the canonical α/β-hydrolase fold (gray). The three areas that have structurally diverged from AChE and JHE are shown (red) as well as the two bundles of α-helices that form the substrate binding cavity (boxed magenta and blue). (*B*) Ribbon diagram of *Lc*αE7, with the structurally different areas colored red and the bundles of α-helices that comprise the substrate cavity boxed in magenta and blue. The phosphorylated serine is shown as spheres. A slice through the surface of the protein is shown alongside to visualize the size of the substrate binding cavity. (*C* and *D*) Ribbon diagrams of AChE [2CSF (50); *T. californica*] and JHE (2FJ0; *M. sexta*), respectively, oriented identically to *Lc*αE7. Bound substrate analogs are represented as spheres. Regions that are not structurally aligned with *Lc*αE7 are colored purple and cyan, respectively. The peripheral and active site binding cavities of AChE are shown as a sliced surface in *C*. The collapsed substrate binding cavity of JHE and the tunnel formed for the leaving group is shown in *D*.

The N terminus also partially occludes the active site entrance (Fig. 2*B*); this occlusion may play a regulatory role, preventing the enzyme from fully functioning until it is in its membrane/lipid-associated state. To test whether the N-terminal helix promotes membrane association, we truncated the gene at position 32 to remove it. This truncation resulted in a large increase in the solubility of the protein as a result of its reduced association with the insoluble (lipidic) fraction (Fig. 3). The cellular location of αE7 in *L. cuprina* and *D. melanogaster*, the presence of a loosely packed amphipathic N-terminal α-helix in the structure, and the marked increase in soluble expression of *Lc*αE7 in *E. coli* as a result of removing this α-helix all strongly suggest that this structural motif is a membrane anchor that is responsible for the membrane/liposome association of this protein.

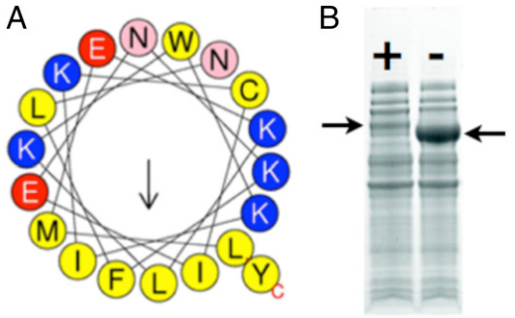

Fig. 3. The N-terminal membrane association helix of *Lc*αE7. (*A*) The helix is amphipathic, with one face being extremely hydrophobic, which is represented as a helical wheel (51). (*B*) Removal of the N-terminal helix results in a vast increase in the soluble expression of the protein in *E. coli* in this 4–20% gradient SDS/PAGE gel. *Lc*αE7 with the N-terminal helix (+) is indicated in *Left*, whereas *Lc*αE7 without the N-terminal helix (–) is indicated in *Right*.

Comparison with Related Proteins. To identify the closest known structural relatives of *Lc*αE7, the structure was submitted to the SAlAmI (structural alignment and match inquiry; http://public.zbh.uni-hamburg.de/salami/) server (19). The results show no close (>30% sequence identity) homolog of *Lc*αE7 exists within known structure databases. The closest relatives with structures in the Protein Data Bank are juvenile hormone esterase (JHE) from the moth *Manduca sexta* (20) and AChE from several species (21) (Fig. 2). Analysis of the ESTHER database, which is dedicated to proteins of the α/β hydrolase fold, reveals that *Lc*αE7 belongs to block C, which includes AChE and JHE, but more specifically belongs to the CBE_B *Arthropoda* family, for which over 800 genes have been described. A detailed comparison (Fig. 2) between *Lc*αE7, JHE, and AChE reveals that the N-terminal α-helix is unique to the α-CBEs, with mature JHE and AChE peptides beginning ~30 aa later. It is also clear that *Lc*αE7 is strikingly similar to both JHE and AChE, with the exception of two small regions that result in large rearrangements of the two subdomains that comprise the substrate binding cavity. First, *Lc*αE7 contains a short antiparallel β-sheet after β1. The analogous region in AChE is the Ω-helix-loop (23), which extends to the active site and forms the choline binding pocket. JHE has a similar extended loop/helix in this position, which effectively closes this part of the substrate cavity, leaving only a small pocket for the acyl group of juvenile hormone. It is clear that the antiparallel β-sheet in *Lc*αE7 results in a much more open active site and creates a groove against which the N-terminal α-helix can pack. Second, *Lc*αE7 has a short helix after α-d that opens the substrate binding cavity further by holding apart the two bundles of α-helices that comprise the cavity. In comparison, JHE lacks this helix, which results in the C-terminal bundle of α-helices collapsing over the active site and closing it but forming a narrow tunnel to the side for the extended juvenile hormone leaving group. In AChE, this region also differs, with the analogous helix coming closer to the active site and forming the gorge, separating the active site from the peripheral substrate

binding site. Overall, this comparison reveals that the active site of *Lc*αE7 is much more open than the active sites of its relatives and shows how small insertions in highly homologous protein structures can have significant impact on the overall topology of substrate binding sites.

Active Site and Natural Substrate Preference. The canonical catalytic triad of the α/β-hydrolase fold is conserved in *Lc*αE7, with Ser218 at the end of β4 hydrogen bonded to His471 at the end of β7, which is, in turn, hydrogen bonded to Glu351 at the end of β6. The structure also reveals the presence of an oxyanion hole consisting of the backbone amide groups of Ala219, Gly136, and Gly137 (Fig. 4). Thus, the catalytic groups in *Lc*αE7 are essentially identical to those groups in most other structural homologs, such as AChE.

The differences and similarities between the active sites of *Lc*αE7, AChE, and JHE were used to identify plausible natural substrates. First, like JHE and AChE, the substrate binding cavity of *Lc*αE7 is also extremely asymmetrical, with a small binding pocket, which is comprised of Phe354, Tyr457, Met460, and Thr472, and a large pocket lined by the side chains of Trp251, Met308, Phe309, Phe355, and Phe421 (Fig. 4). This asymmetry strongly suggests that, like juvenile hormone and acetylcholine, the carboxylesters that *Lc*αE7 hydrolyzes most likely have an acyl group. Second, unlike AChE but like JHE, the binding cavity is almost entirely hydrophobic, suggesting that the leaving acid group will be strongly hydrophobic. Additionally, its association with the fat droplet (6, 17) limits the possible esters that it may encounter to triglycerides, cholesterol esters, retinyl esters, and fatty acid methyl esters (FAMEs) (Fig. 1*B*) (24). Of these esters, retinyl esters and triglycerides are far too large for the binding pocket. Thus, cholesterol acetate and FAMEs were tested as substrates. No activity was observed with cholesterol acetate, consistent with the curved shape of the pocket making it unsuited for substrates with long rigid leaving groups. Docking analysis suggested that the active site is ideally shaped for FAMEs of medium length (Fig. 4). *Lc*αE7 efficiently catalyzed the hydrolysis of these compounds with high-specificity constants (up to 1.4×10^6 M^{-1} s^{-1} for methyl decanoate) (Table 2). A specificity constant in the order of 10^6 M^{-1} s^{-1} is highly indicative of a natural substrate, especially in metabolic scenarios (25). This finding is also in keeping with a role in lipid metabolism and the observation that *Md*αE7-null *Musca domestica* KOs are deficient in fatty acid accumulation (6).

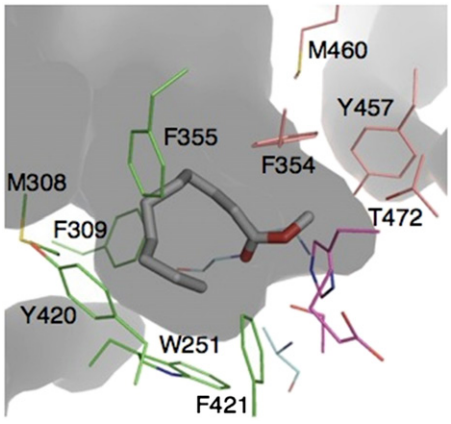

Fig. 4. The substrate binding pocket of *Lc*αE7. The pocket can be divided into sections: a small pocket (pink) comprising Y457, M460, F354, and T472 and a larger pocket (green) comprising F355, Y420, W251, M308, F309, and F421. The FAME methyl decanoate has been docked in the active site. The catalytic triad is colored magenta, and the oxyanion hole is colored sky blue.

Structural Basis for OP Resistance. CBEs, such as *Lc*αE7, that belong to the *αEsterase* gene cluster are known to provide protection against OPs, even as WT enzymes (6). Both AChE and *Lc*αE7 are inhibited by OPs as a result of phosphorylation of the catalytic serine. However, although this process is often irreversible in AChE as a result of a secondary aging reaction, in which the phosphorylated serine is dealkylated (26), *Lc*αE7 is capable of hydrolytic turnover of OPs at significant, albeit low, rates (Table 2) (27). To investigate why this process does not occur in *Lc*αE7, we captured *Lc*αE7 in its intermediate, phosphorylated state by flash-cooling crystals of *Lc*αE7 that had been soaked in 1 mM diethyl 4-methylumbelliferyl phosphate. These crystals diffracted to 1.8 Å (Table 1), and as shown in Fig. 5 and Fig. S5, no evidence of aging was observed (27). This finding is consistent with previous work that has shown mammalian CBEs to be resistant to the aging reaction (28, 29).

Aging of AChE, involving dealkylation of the phosphorylated serine, has been proposed to occur through either hydrolysis or carbocation bond scission (26, 30). To investigate why *Lc*αE7 is resistant to aging, we compared the structural features that are known to make AChE prone to aging (Fig. 5) (26, 30–32). First, activation and stabilization of the alkyl side chain is thought to involve the catalytic histidine, which is positioned close to the alkyl side chain and stabilized in a position to allow this interaction by Glu199 and Phe331 (*Torpedo californica* AChE numbering). In comparison, the catalytic histidine (His471) in *Lc*αE7 is farther away from the alkyl side chain (3.2 vs. 2.5 Å) and not well-oriented to interact with this group during dealkylation; the catalytic histidine in human CBE is also poorly positioned to interact with the alkyl side chain of a phosphoylated serine (28). Although Glu217 is present in a similar position to Glu199 in AChE, there is no residue present in *Lc*αE7 in the same position as Phe331 in AChE, meaning that the catalytic histidine cannot be stabilized in the required position to catalyze dealkylation. Second, the Ω-loop of AChE, containing Trp84, is known to play an essential role in catalysis of acetylcholine hydrolysis and aging through cation-π interactions between the choline or carbocation leaving group and the indole moiety of Trp84 (23, 30). Like Phe331, this residue is not present in *Lc*αE7; the Ω-loop is, in fact, replaced by the short antiparallel sheet after strand β1 (Fig. 2 *B* and *C*). In *Lc*αE7, a tyrosine residue (Tyr427) is present in a similar position, but the electronegative hydroxyl substitution weakens the cation-π interaction in contrast to the substituted indole, which is known to be particularly activated (33).

Therefore, the ability of *Lc*αE7 to confer OP resistance derives from two structural properties. First, the immediate active site of *Lc*αE7 is strikingly similar to AChE (Fig. 5) and highly complementary to OPs. Indeed, studies have shown that the binding affinity of *Lc*αE7 for the OP paraoxon is ∼10-fold higher than the binding affinity of *Lc*AChE (22 vs. 244 nM) (4, 34). Second, specific residues required for the aging reaction to occur in AChE (Trp84 and Phe331) are absent in *Lc*αE7, allowing for slow turnover of the OP rather than irreversible inhibition. The differential cost to the organism of *Lc*αE7 vs. AChE inhibition is also important; although AChE is essential, loss of αE7 CBE activity in *D. melanogaster* and *L. cuprina* is tolerated (6, 35). Additionally, αE7 CBEs are expressed in relatively high abundance across the larvae and adult life stages during which

Table 2. Kinetic parameters for substrate turnover by *Lc*αE7

Substrate	k_{cat}/K_M (10^6 M^{-1} s^{-1})
Methyl hexanoate	0.28 ± 0.02
Methyl octanoate	0.83 ± 0.07
Methyl decanoate	1.38 ± 0.02
Methyl laurate	0.2 ± 0.03
Methyl myristate	0.061 ± 0.001
Diethyl 4-methylumbelliferyl phosphate	0.05 ± 0.005

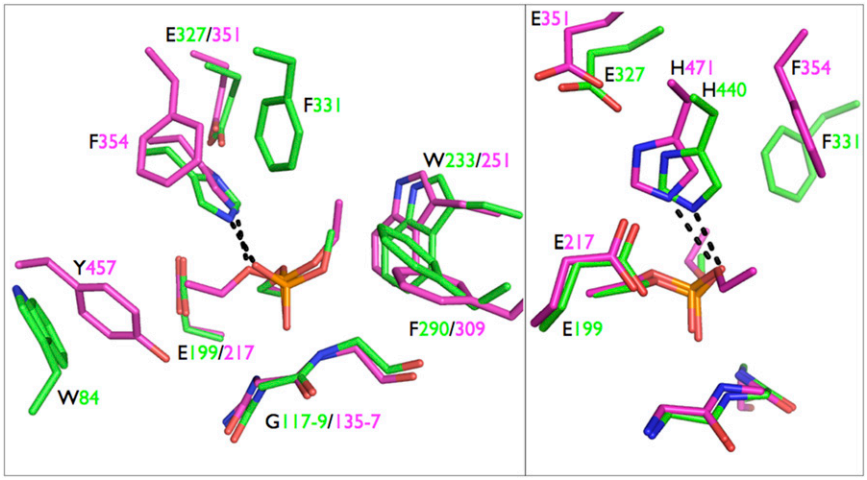

Fig. 5. Comparison between *Lc*αE7-diethylphosphate (magenta) and AChE-methylphosphate (green) after aging of AChE-dimethylphosphate (3GEL; *T. californica*). *Right* is rotated 90° from *Left*. The active sites and substrate binding sites are generally highly conserved. The key differences between the structures include the closer distance (2.7 vs. 3.2 Å) between H440 and the side chain oxygen of the adduct in AChE, the absence of a residue at an analogous position to AChE F331 in *Lc*αE7, and the replacement of W84 in AChE by Y457 in *Lc*αE7.

the insects will be exposed to insecticides (36, 37). Their abundant expression allows αE7 CBEs to act as scavengers for OPs, sequestering the poison and slowly detoxifying it. Although the turnover rates of OPs by *Lc*αE7 are currently much lower than other enzymes that have been engineered for OP hydrolysis (38), its high affinity for OPs makes *Lc*αE7 a good starting point for the development of a high-specificity enzyme for OP poisoning. Indeed, in its native host, the G137D mutation is seen to increase the rate of OP turnover by two orders of magnitude, resulting in a large protective effect (4).

Conclusion

Hundreds of studies have been published on CBE-mediated OP resistance since the discovery of this phenomenon by Openoorth and van Apseren in 1960 (39). This first structure of an insect CBE has allowed us to identify a probable natural substrate for the enzyme, and it revealed the molecular basis for the ability of insect CBEs to hydrolyze and detoxify OP insecticides. This work shows the power of laboratory evolution for generating slightly modified versions of important proteins that can be heterologously expressed in *E. coli* at high levels and more easily studied and crystallized, allowing their molecular structures to be solved.

Materials and Methods

All chemicals were purchased from Sigma-Aldrich unless otherwise specified.

Cloning and Laboratory Evolution. The internal NdeI restriction site in the WT *LcαE7* gene was removed using primers E31 and E32 (Table S1) before the gene was cloned into the pETMCSIII vector (40) between the NdeI (New England Biolabs) and EcoRI (New England Biolabs) sites using the E33 and E34 primers (Table S1). Random mutations were introduced to the coding region of *LcαE7* by error-prone PCR. Briefly, the PCR was performed using primers pET1 and pET2, Taq DNA polymerase buffer (New England Biolabs), 5 mM $MgCl_2$, 0.1–0.4 mM $MnCl_2$, 0.5 mM dNTPs (New England Biolabs), 5 U Taq DNA polymerase (New England Biolabs), and milliQ H_2O to a final volume of 50 μL. Thermocycling was performed with 30 cycles of 94 °C (10 s), 45 °C (10 s), and 72 °C (30 s). The PCR product was digested with NdeI, and EcoRI-digested PCR product was gel extracted, ligated into pETMCS III, and then used to transform BL21 (DE3)-competent cells (Invitrogen).

For library screening, ~100,000 colonies were plated onto LB-agar plates supplemented with 100 μg/mL ampicillin. Colonies were blotted onto Whatman grade 3 filter paper (GE Healthcare) and incubated for 1 h at 50 °C (increased to 55 °C, 60 °C, and 70 °C for the subsequent generations). The residual esterase activity was assayed by spraying heat-treated colonies with substrate solution, which consisted of 0.8% (wt/vol) Fast Red, 10 mM β-naphthyl acetate, and 100 mM Tris (pH 7.0). The most stable mutants were identified as those colonies that produced the most intense red color. A secondary screen of the best variants was carried out, in which the best variants from the plate screen were picked and grown in 96-deep well plate formats. The overnight cultures were heat stressed for 1 h at the same temperatures used in the primary screen, and 25 mL overnight cultures were assayed using a Molecular Devices plate reader at 490 nm in the presence of 0.5 mM β-naphthyl acetate, 0.5 mM Fast Red dye, and 100 mM Tris (pH 7.0). The best 5–10 variants of each generation were carried forward to the next generation, and the final product *Lc*αE7-4 was sequenced at the Micromon Sequencing Facility, Melbourne, Australia.

Protein Expression and Purification. WT and mutant *LcαE7* were expressed in *E. coli* BL21-DE3 (Invitrogen) cells grown at 30 °C overnight in Overnight Express TB Media (Merck) supplemented with 100 μg/mL ampicillin. Cells were pelleted at 5,000 × *g* and lysed using 1× Bugbuster protein extraction reagent (Merck) in 100 mM Tris·Cl (pH 8) and 200 mM NaCl. Lysate was filtered and passed over a 5-mL Ni-NTA column (Qiagen), and protein was eluted using lysis buffer supplemented with 500 mM imidazole. SDS/PAGE analysis of pooled active fractions indicated that purified *LcαE7* was essentially homogeneous. The active fraction was then subjected to size exclusion chromatography in 20 mM Hepes (pH 7.5) and 50 mM NaCl using a Sephacryl S300 column (GE Healthcare). Protein concentration was determined by measuring absorbance at 280 nm using an extinction coefficient of 91,510 M^{-1} cm^{-1} calculated using the Protparam server (41) (none of the mutations in *LcαE7*4-1 affect absorbance at 280 nm).

Enzyme Assays. ***FAME assays.*** FAMEs were purchased in the highest available purity. The reaction mixture (200 μL) consisted of substrate (200 μM) and enzyme in 25 mM Tris·HCl (pH 8.0) supplemented with 0.2% BSA and 0.01% gum arabic as an emulsifying agent. The reaction mix was emulsified by sonication for 5 min in a water bath. The reaction was carried out in a silanized screw-top vial (Agilent) at 25 °C and quenched at specific time points with equivalent amounts of ice-cold hexane (containing 250 μm heptanone as an external standard). The tubes were then placed in a vortex shaker for 15 min at maximum speed (MS1 minishaker; IKA). The upper (hexane) layer was then carefully transferred with a glass pipette to a deactivated glass insert (Agilent) for analysis with an Agilent 7890 series GC/MS and GC with flame ionization detection. The system also consisted of an Agilent 597 series MSD standalone capillary detector together with a CTC PAL autosampler (G6500 Combi PAL; CTC Analytics AG). The compounds were separated on a J&W DB-WAX column (30 m × 0.25 mm × 0.25 μm; Agilent Technologies) with He (2 mL/min) as the carrier gas. The oven temperature was initially set at 50 °C for 2 min, then subsequently increased over a gradient of 10 °C to 250 °C, and held for 5 min. The injector and detector temperatures were set at 250 °C with a 15:1 split ratio. Quantities of FAMEs were calculated using response factors as per standard protocol. All assays were conducted in duplicate or triplicate. Apparent k_{cat}/K_M values were estimated using Eq. **1**:

$$k_{cat}/K_M^{app} = v_o/([E]/[S]). \quad [1]$$

OP and carboxylester assays. Purified enzymes were incubated with substrates (diethyl 4-methylumbelliferyl phosphate and 4-nitrophenyl acetate) in 100 mM Hepes (pH 8.0) and 100 mM NaCl. The rate at which the substrates were hydrolyzed was determined by monitoring product formation using a molecular devices 96-well plate reader. For 4-nitrophneyl acetate, the assay was followed at 405 nm, and product concentration was determined using a molar extinction coefficient (ε = 14,800 M^{-1} cm^{-1}). For diethyl 4-methylumbelliferyl

phosphate, the product fluorescence was followed at λ_{ex} = 360 nm and λ_{emm} = 455 nm, and product concentration was determined through calculation of a standard curve of 4-methylumbelliferone in the assay buffer. The k_{cat} and K_M values were determined by fitting the initial velocity data to the Michaelis–Menten equation. Assays were conducted in duplicate.

Crystallization, Structure Determination, Substrate Soaking, and Docking. Crystals of *Lc*αE74 were grown using the hanging-drop vapor diffusion method, with reservoir solutions of 100 mM Mes (pH 6.5) and 20% PEG 2K MME or 100 mM sodium-acetate (pH 4.6) and 20% PEG 2K MME. The concentration of PEG 2K MME was increased to 35% for use as a cryoprotectant during flash cooling to 100 K of the crystals under a stream of nitrogen gas. Diffraction data were collected at beamlines ID 14–4 and 23–2 of the European Synchrotron Radiation Facility with wavelengths of 0.9393 and 0.8266 Å. Diffraction data were indexed, integrated, and scaled using the XDS package (42). Data collection statistics are shown in Table 1. Phases were obtained using molecular replacement with the program *MOLREP* and structure of mouse AChE (13). Iterative model building was performed using *COOT* (43) and *BUCCANEER* (44). Refinement (including twin refinement) was undertaken using *REFMAC* (45), which was implemented in the *CCP4* suite of programs (46).

Crystals *Lc*αE7-4 from pH 4.6 conditions were soaked with 1 mM diethyl 4-methylumbelliferyl phosphate for time periods between 1 h and 3 d before data collection. The presence of the ligand was confirmed through investigation of omit electron density maps. Input structures for docking were generated with the AutoDock Tools package (47), and rigid docking was performed using Autodock Vina (48). The searching space was centered on the catalytic serine, and a search box of 36 × 52 × 48 Å was used to encompass the entire substrate binding cavity. All protein structure images were produced using PyMol (25). Protein structure diagrams were produced using *TOPDRAW* (49).

ACKNOWLEDGMENTS. This work was supported by Defense Threat Reduction Agency Contract HDTRA1-11-C-0047. C.J.J. was supported by a Marie Curie International Incoming Fellowship.

1. Grube A, Donaldson D, Kiely T, Wu L (2011) *Pesticide Industry Sales and Usage* (United States Environmental Protection Agency, Washington, DC).
2. Whalon ME, Mota-Sanchez D, Hollingworth RM, eds (2008) *Global Pesticide Resistance in Arthropods* (CAB International, Oxfordshire, United Kingdom).
3. Jackson CJ, Oakeshott JG, Sanchez-Hernandez J, Wheelock C (2010) Carboxylesterases in the metabolism and toxicity of pesticides. *Acetylcholinesterase Pesticides: Metabolism, Neurotoxicity and Epidemiology*, eds Satoh T, Gupta RC (Wiley, New York), pp 57–77.
4. Newcomb RD, et al. (1997) A single amino acid substitution converts a carboxylesterase to an organophosphorus hydrolase and confers insecticide resistance on a blowfly. *Proc Natl Acad Sci USA* 94(14):7464–7468.
5. Marrs TC (1993) Organophosphate poisoning. *Pharmacol Ther* 58(1):51–66.
6. Birner-Gruenberger R, et al. (2012) Functional fat body proteomics and gene targeting reveal in vivo functions of Drosophila melanogaster α-Esterase-7. *Insect Biochem Mol Biol* 42(3):220–229.
7. Campbell PM, Newcomb RD, Russell RJ, Oakeshott JG (1998) Two different amino acid substitutions in the ali-esterase, E3, confer alternative types of organophosphorus insecticide resistance in the sheep blowfly, Lucilia cuprina. *Insect Biochem Mol Biol* 28(3):139–150.
8. Campbell PM, et al. (2003) Developmental expression and gene/enzyme identifications in the alpha esterase gene cluster of Drosophila melanogaster. *Insect Mol Biol* 12(5):459–471.
9. Healy MJ, Dumancic MM, Oakeshott JG (1991) Biochemical and physiological studies of soluble esterases from Drosophila melanogaster. *Biochem Genet* 29(7–8):365–388.
10. Tweedie S, et al. (2009) FlyBase: Enhancing Drosophila Gene Ontology annotations. *Nucleic Acids Res* 37(Database issue):D555–D559.
11. Beller M, et al. (2006) Characterization of the Drosophila lipid droplet subproteome. *Mol Cell Proteomics* 5(6):1082–1094.
12. Ranson H, et al. (2002) Evolution of supergene families associated with insecticide resistance. *Science* 298(5591):179–181.
13. Bourne Y, Taylor P, Marchot P (1995) Acetylcholinesterase inhibition by fasciculin: Crystal structure of the complex. *Cell* 83(3):503–512.
14. Carr PD, Ollis DL (2009) α/β hydrolase fold: An update. *Protein Pept Lett* 16(10):1137–1148.
15. Krissinel E, Henrick K (2007) Inference of macromolecular assemblies from crystalline state. *J Mol Biol* 372(3):774–797.
16. Ishikawa K, Nakamura H, Morikawa K, Kanaya S (1993) Stabilization of Escherichia coli ribonuclease HI by cavity-filling mutations within a hydrophobic core. *Biochemistry* 32(24):6171–6178.
17. Spackman ME, Oakeshott JG, Smyth KA, Medveczky KM, Russell RJ (1994) A cluster of esterase genes on chromosome 3R of Drosophila melanogaster includes homologues of esterase genes conferring insecticide resistance in Lucilia cuprina. *Biochem Genet* 32(1–2):39–62.
18. Pierleoni A, et al. (2011) MemPype: A pipeline for the annotation of eukaryotic membrane proteins. *Nucleic Acids Res* 39(Web Server issue):W375–W380.
19. Margraf T, Schenk G, Torda AE (2009) The SALAMI protein structure search server. *Nucleic Acids Res* 37(Web Server issue):W480–W484.
20. Wogulis M, et al. (2006) Structural studies of a potent insect maturation inhibitor bound to the juvenile hormone esterase of Manduca sexta. *Biochemistry* 45(13):4045–4057.
21. Sussman JL, et al. (1991) Atomic structure of acetylcholinesterase from Torpedo californica: A prototypic acetylcholine-binding protein. *Science* 253(5022):872–879.
22. Lenfant N, et al. (2013) ESTHER, the database of the α/β-hydrolase fold superfamily of proteins: Tools to explore diversity of functions. *Nucleic Acids Res* 41(Database issue):D423–D429.
23. Velan B, et al. (1996) Structural modifications of the omega loop in human acetylcholinesterase. *FEBS Lett* 395(1):22–28.
24. Gilbert LI, Chino H (1974) Transport of lipids in insects. *J Lipid Res* 15(5):439–456.
25. Bar-Even A, et al. (2011) The moderately efficient enzyme: Evolutionary and physicochemical trends shaping enzyme parameters. *Biochemistry* 50(21):4402–4410.
26. Nachon F, Asojo OA, Borgstahl GE, Masson P, Lockridge O (2005) Role of water in aging of human butyrylcholinesterase inhibited by echothiophate: The crystal structure suggests two alternative mechanisms of aging. *Biochemistry* 44(4):1154–1162.
27. Heidari R, et al. (2004) Hydrolysis of organophosphorus insecticides by in vitro modified carboxylesterase E3 from Lucilia cuprina. *Insect Biochem Mol Biol* 34(4):353–363.
28. Fleming CD, et al. (2007) Crystal structures of human carboxylesterase 1 in covalent complexes with the chemical warfare agents soman and tabun. *Biochemistry* 46(17):5063–5071.
29. Maxwell DM, Brecht KM (2001) Carboxylesterase: Specificity and spontaneous reactivation of an endogenous scavenger for organophosphorus compounds. *J Appl Toxicol* 21(1 Suppl 1):S103–S107.
30. Shafferman A, et al. (1996) Aging of phosphylated human acetylcholinesterase: Catalytic processes mediated by aromatic and polar residues of the active centre. *Biochem J* 318(Pt 3):833–840.
31. Carletti E, et al. (2008) Aging of cholinesterases phosphylated by tabun proceeds through O-dealkylation. *J Am Chem Soc* 130(47):16011–16020.
32. Millard CB, et al. (1999) Crystal structures of aged phosphonylated acetylcholinesterase: Nerve agent reaction products at the atomic level. *Biochemistry* 38(22):7032–7039.
33. Dougherty DA (1996) Cation-pi interactions in chemistry and biology: A new view of benzene, Phe, Tyr, and Trp. *Science* 271(5246):163–168.
34. Chen Z, Newcomb R, Forbes E, McKenzie J, Batterham P (2001) The acetylcholinesterase gene and organophosphorus resistance in the Australian sheep blowfly, Lucilia cuprina. *Insect Biochem Mol Biol* 31(8):805–816.
35. McKenzie J, O'Farrell K (1993) Modification of developmental instability and fitness: Malathion-resistance in the Australian sheep blowfly *Lucilia cuprina*. *Genetica* 89(3):67–76.
36. Parker AG, Campbell PM, Spackman ME, Russell RJ, Oakeshott JG (1996) Comparison of an esterase associated with organophosphate resistance in Lucilia cuprina with an orthologue not associated with resistance in Drosophila melanogaster. *Pestic Biochem Physiol* 55(2):85–99.
37. Parker AG, Russell RJ, Delves AC, Oakeshott JG (1991) Biochemistry and physiology of esterases in organophosphate-susceptible and -resistant strains of the Australian sheep blowfly, Lucilia cuprina. *Pestic Biochem Physiol* 41(3):305–318.
38. Goldsmith M, et al. (2012) Evolved stereoselective hydrolases for broad-spectrum G-type nerve agent detoxification. *Chem Biol* 19(4):456–466.
39. Oppenoorth FJ, van Asperen (1960) Allelic genes in the housefly producing modified enzymes that cause organophosphate resistance. *Science* 132(3422):298–299.
40. Neylon C, et al. (2000) Interaction of the Escherichia coli replication terminator protein (Tus) with DNA: A model derived from DNA-binding studies of mutant proteins by surface plasmon resonance. *Biochemistry* 39(39):11989–11999.
41. Gasteiger E, et al. (2005) Protein identification and analysis tools on the ExPASy Server. *The Proteomics Protocols Handbook*, ed Walker JM (Humana Press, Clifton, NJ), pp 571–607.
42. Kabsch W (2010) XDS. *Acta Crystallogr D Biol Crystallogr* 66(Pt 2):125–132.
43. Emsley P, Lohkamp B, Scott WG, Cowtan K (2010) Features and development of Coot. *Acta Crystallogr D Biol Crystallogr* 66(Pt 4):486–501.
44. Cowtan K (2006) The Buccaneer software for automated model building. 1. Tracing protein chains. *Acta Crystallogr D Biol Crystallogr* 62(Pt 9):1002–1011.
45. Murshudov GN, et al. (2011) REFMAC5 for the refinement of macromolecular crystal structures. *Acta Crystallogr D Biol Crystallogr* 67(Pt 4):355–367.
46. Collaborative Computational Project, Number 4 (1994) The CCP4 suite: Programs for protein crystallography. *Acta Crystallogr D Biol Crystallogr* 50(Pt 5):760–763.
47. Morris GM, et al. (2009) AutoDock4 and AutoDockTools4: Automated docking with selective receptor flexibility. *J Comput Chem* 30(16):2785–2791.
48. Trott O, Olson AJ (2010) AutoDock Vina: Improving the speed and accuracy of docking with a new scoring function, efficient optimization, and multithreading. *J Comput Chem* 31(2):455–461.
49. Bond CS (2003) TopDraw: A sketchpad for protein structure topology cartoons. *Bioinformatics* 19(2):311–312.
50. Colletier JP, et al. (2006) Structural insights into substrate traffic and inhibition in acetylcholinesterase. *EMBO J* 25(12):2746–2756.
51. Gautier R, Douguet D, Antonny B, Drin G (2008) HELIQUEST: A web server to screen sequences with specific alpha-helical properties. *Bioinformatics* 24(18):2101–2102.